PAPER

Check for updates

SiO$_2$ thin film growth through a pure atomic layer deposition technique at room temperature†

D. Arl, [ID]* V. Rogé, N. Adjeroud, B. R. Pistillo, [ID] M. Sarr, N. Bahlawane [ID]
and D. Lenoble

In this study, less contaminated and porous SiO$_2$ films were grown *via* ALD at room temperature. In addition to the well-known catalytic effect of ammonia, the self-limitation of the reaction was demonstrated by tuning the exposure of SiCl$_4$, NH$_3$ and H$_2$O. This pure ALD approach generated porous oxide layers with very low chloride contamination in films. This optimized RT-ALD process could be applied to a wide range of substrates that need to be 3D-coated, similar to mesoporous structured membranes.

Introduction

Silicon dioxide (SiO$_2$) and more generally ultra-thin oxide films have been extensively described as good components for modern nanotechnologies such as dielectric materials in silicon microelectronic devices,[1,2] anticorrosion films[3] or non-exhaustive applications of nanoscale films in catalysis. The environment- and human-friendly nature of SiO$_2$ induces its wide use in protective layers for antisticking, antifogging, self-cleaning or water repellency.[4–7] Various techniques such as chemical vapor deposition,[8] lithographic patterning,[9] electro-chemical deposition[10] or sol–gel[11,12] were investigated to prepare superhydrophobic SiO$_2$ by tuning surface roughness or energy. SiO$_2$ is consistently known for its application in protective or gate insulator coatings[13] and interfacing high-*k* (ref. 14–19) or surface passivation materials.[20–23] The increased demand for transparent active materials at the nanoscale justify the need for a deposition technique compatible with sensitive pre-deposited underlying layers, flexible plastic devices or high aspect ratio substrates.[24–28] Therefore, atomic layer deposition (ALD) is considered as one of the most suitable techniques for its performance in terms of sub-nanometer thickness control and penetration coating into deep trenches or mesoporous structures.

SiO$_2$ thin films obtained through ALD have widely been described as binary surface reactions dealing with various types of precursors Si(C$_2$H$_5$O)$_4$,[29] SiCl$_4$ (ref. 13 and 30–33) or Si(NCO)$_4$ (ref. 34) with H$_2$O; CH$_3$OSi(NCO)$_3$ (ref. 35 and 36) with H$_2$O$_2$; Si(NCH$_3$)$_2$)$_4$, ((CH$_3$)$_2$N)$_3$SiH[37] or SiH$_2$(NEt$_2$)$_2$ (ref. 38)). Besides the necessity to work at high temperatures (*i.e.* >100–350 °C), most of the reactions require large reactant exposure of ≥10^9 L

(1 L = 10^{-6} Torr s) with a growth rate of[59] ∼1–2 Å per cycle.[39] One approach to decrease the deposition temperature and the level of contamination is to use plasma-enhanced-ALD (PE-ALD).[40,58,59] It is possible to decrease the temperature below 50 °C, and these SiO$_2$ films are described as excellent candidates for thin film encapsulation in organic devices or TFT gate insulators due to the absence of impurities and good electrical properties.[41–43,60] Currently, the use of amino ligands as precursors leads to promising results, even on large surfaces; however, a final annealing step at 900–1000 °C is required to decrease interface defects or carbon contamination.[44,45] Many efforts have been done, in terms of parameters and choice of precursors, in order to optimise ALD process, for the growth of SiO$_2$ coatings at high temperatures. Nevertheless, it is commonly agreed that there is a strong interest in the development of the process at room temperature. George *et al.* described the atomic layer-controlled growth using SiCl$_4$ and H$_2$O many times.[13,31,44,46] They demonstrated that a reaction catalyzed using Lewis bases such as pyridine (C$_5$H$_5$N) or ammonia (NH$_3$) avoids large precursor flow rates and can only occur close to room temperature. Nevertheless, in these studies, C$_5$H$_5$N or NH$_3$ were never really considered as "precursors". The proposed mechanism, which took into account the hydrogen bonding between the Lewis base and either the SiOH* surface species or the H$_2$O reactant, was studied by considering the global residual pressure of the continuous flow of the catalyst. Moreover, the secondary reaction of the catalyst reservoir (continuous flow), available in the reactor with HCl as the byproduct, drastically increased the probability of the inclusion of contaminants in the film. Therefore, a sequential approach could enhance the quality of the film and the understanding of the role of the catalyst.

This paper describes a pure ALD study of SiO$_2$ using the optimized sequential exposure of SiCl$_4$, H$_2$O and NH$_{3(g)}$ precursors at room temperature. The ALD mode was confirmed by tuning the exposition of each precursor and the related

Luxembourg Institute of Science and Technology, 41 rue du Brill, L-4422, Luxembourg. E-mail: didier.arl@list.lu

purges. The initiation of the exposition was followed by using the residual gas analysis (RGA) mass spectrometer. Atomic growth control was investigated by the *in situ* Quartz Crystal Microbalance (QCM) and X-ray Photoelectron Spectroscopy (XPS), Dynamic-Secondary Mass Ion Spectroscopy (D-SIMS) and X-ray Diffraction (XRD) post-characterizations. A comparison between our investigation and the state-of-the-art of low temperature ALD SiO$_2$ synthesis revealed the possibility to deposit ultra-thin films with very low contaminations at room temperature. The film conformality is shown and the capability of this optimized binary reaction, to be used on various types of temperature-sensitive supports with high aspect ratios, is confirmed.

Materials and methods

ALD processes were carried out in a TFS200-Beneq reactor in the planar configuration at a base pressure of 0.3 mbar. SiO$_2$ thin films were then deposited on Si substrates, preliminary prepared by a standardized cleaning procedure established by Radio Corporation of America (RCA). The deposition reactor was equipped with a QCM (Neyco) for the gravimetric monitoring of the film growth. The QCM was fixed to the central part of the substrate holder. A quadrupole mass spectrometer, Vision-2000C, MKS-instrument, was assembled at the outlet of the deposition reactor to monitor the exhaust gas composition. SiO$_2$ thin films were obtained at room temperature using SiCl$_4$ and H$_2$O as precursors. The vaporized precursors were transferred to the ALD reaction chamber with N$_2$ as the carrier gas. SiCl$_4$ was purchased from Sigma Aldrich and used as-received. Both canisters containing the precursors were maintained at 19 °C during deposition. NH$_3$ gas (<99.9%), used as a catalyst, was injected into the reactor under 1 bar pressure.

The morphology and thickness of the obtained samples were characterized using a FEI Heliosnanolab 650 Focused Ion Beam Secondary Electron Microscope (FIB-SEM). The structure of the films deposited on dedicated Kapton tape was probed by small-angle X-ray scattering (SAXS) using an X-ray Diffractometer (X'Pert Pro (Panalytical)) equipped with a focusing mirror and a Pixcel 1D detector in the transmission mode. The elemental composition depth profile was assessed using D-SIMS (Cameca, IMSLAM); however, the quantification was performed by XPS (Thermo VG Scientific, MicroLab 350) using Al Kα source.

Results and discussion

Catalytic SiO$_2$ RT-ALD growth

SiO$_2$ films obtained at room temperature have already been prepared by the sequential exposure (ABAB...) of two reactants (A and B). Many well-known precursors require high deposition temperatures, plasma or highly reactive co-reactants such as ozone gas.[47] Despite a low enthalpy of reaction, SiCl$_4$ usually reacts with water (oxidant species) at high temperatures (>325 °C).[13] The comparison of thermal ALD and room temperature processes reveals a higher growth rate/ALD cycle in favour of room temperature reactions (~2 Å per cycle) (Fig. S1, ESI†).

The amount of contaminants integrated in RT-SiO$_2$ films is inherently dependent on the way of tuning the surface exposure to precursors. Based on studies by George *et al.*,[31] we investigated the growth of SiO$_2$ at room temperature (RT)-ALD by alternatively exposing the surface to SiCl$_4$ and H$_2$O under a constant flow of NH$_3$. The exposure time was fixed at 90 s for SiCl$_4$ with a purge time of 1 min. H$_2$O exposure was fixed at 90 s with a purge time of 5 min to ensure a perfect saturation of the surface.[31] The *in situ* monitoring of the film growth obtained by the QCM is shown in Fig. S2, ESI.† As already described,[31] the reduction reaction of SiCl$_4$ with water is depicted through the minimum of SiCl$_4$ weight gain (Fig. S2b, ESI†) and the longer reaction of the NH$_3$–H$_2$O mixture (Fig. S2c–e, ESI†). Then, as shown in Fig. S2b, ESI,† the gain of mass that is observed in one ALD cycle is predominantly obtained from the half reaction of H$_2$O. Nevertheless, the growth rate of ~1.5 Å per cycle (297 nm/ 2000 cycles), experimentally obtained through this process with a constant flow of NH$_3$, tends to reach the 2 Å per cycle value described by George *et al.*[31]

XPS elemental analysis of the SiO$_2$ film (deposited on Al$_2$O$_3$/ Si) (Fig. 1) shows the presence of carbon, nitrogen and chlorine in addition to silicon and oxygen within the SiO$_2$ deposited film. A depth profiling analysis reveals that the carbon is restricted to the surface of the film.

The asymmetry of the C 1s peak suggests the presence of C–H, C–O–C or C=O bonds at the surface due to air exposure. The Si 2p peak of the Si–O layer appeared at 104.4 eV with a 1.77 eV (broadened up to 2.22 eV due to charge effects during the depth profiling) full width at half maximum (FWHM). The sharp and symmetric Si 2p peak centred at ~104 eV suggests an oxidation state of +1, which was attributed to the presence of SiO$_2$. A high contribution of the byproducts of the reaction is detected through the presence of Cl and N elements in the films. The Si/ Cl ratio increased from ~1.3 at the surface to 3.2 in the bulk of the film (Table 1).

Furthermore, the reaction of the lone pair of active –Cl with the hydrogen of water induced a significant formation of HCl. The higher detection limit of D-SIMS was used to screen the chemical elements present in the "bulk" of the film, particularly
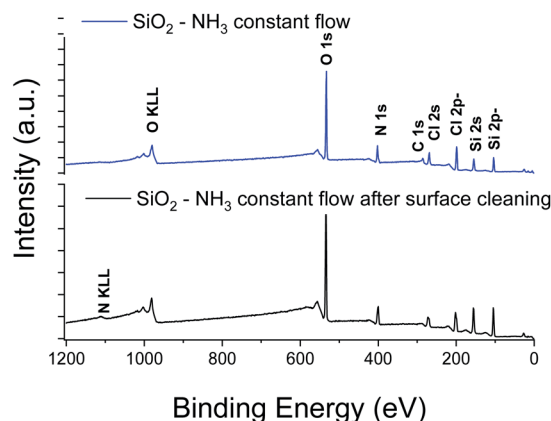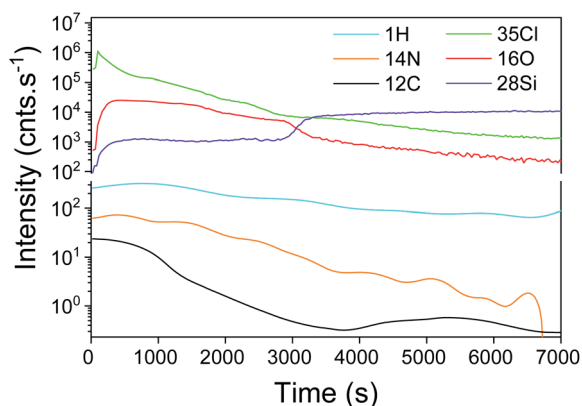

Fig. 1 XPS survey spectra of SiO$_2$ thin films obtained with a constant flow of NH$_3$.

Table 1 XPS quantification of elements present in the SiO_2 thin film obtained with a constant flow of NH_3

| Name	At%	At% (depth profiling)
Si 2p	17.6	29.5
O 1s	45.9	47.7
N 1s	16.5	13.5
Cl 2p	13.6	9.1
C 1s	6.4	<1

Fig. 2 SIMS depth profile of the SiO_2 film obtained with a constant flow of NH_3. A thickness of 297 nm is calculated by the sputtering time.

for light elements such as hydrogen. As shown in Fig. 2, all typical elements of the deposited film, *i.e.* Si, O, Cl, N, H and C, are detected. The intensity of Cl is similar to that of Si and O while a difference in the intensity is observed for H, N and C. It can be seen from the depth profile analysis that the signal of C decreases rapidly, which is in agreement with the XPS results. As H% is roughly constant, the slow decrease in N and Cl tends to confirm that a part of the film is composed of NH_4Cl contaminants.

Contaminant inclusion mechanism

George *et al.* described the mechanism of a catalysed binary reaction that spontaneously takes place in the presence of pyridine or NH_3 as a Lewis base agent.[30,48] The hydrogen bonding between the Lewis base and SiOH* (surface species) or H_2O allows the reaction to be performed at room temperature (Fig. S3, ESI†). Compared to high temperature processes that use large precursor exposures (>10^3 Torr s), SiO_2 RT-ALD takes place owing to the strong nucleophilic attack of the oxygen from (i) Si<u>O</u>H* on $SiCl_4$ and that from (ii) H_2O on SiCl*.[46] Nevertheless, to the best of our knowledge, no specific data have been reported on the variation of the chemical composition and the morphology of such films. Based on the catalytic effect of NH_3, it can be clearly deduced that a constant flow of NH_3 statistically ensures a maximized reaction of –O on all –O–Si–(Cl)$_n$ available sites. Nevertheless, the perfect delimitation of the exposure windows at room temperature could be enhanced by working in a non-conventional high vacuum state (<10^{-6} Torr). As it is not

the case for standard ALD reactors, we attempted to understand and control the contaminant inclusion mechanism in the pulsed NH_3 regime. Thus, the state-of-the-art production of SiO_2 at RT using a constant flow of NH_3 has been compared to pulse NH_3-catalysed RT-ALD. Inspired by the reactivity of chlorinated precursors described by Damyanov *et al.*,[49] the amount of contamination could be cautiously explained by the functionality x of the adsorbed species at the surface explained hereafter:

$$x(\equiv Si–OH) + SiCl_4 \rightarrow (\equiv Si–O)_x SiCl_{4-x} + xHCl$$
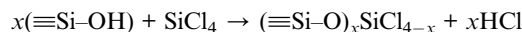
$x = 1$: monofunctional, $x = 2$: bifunctional and $x = 3$: trifunctional.

The injected precursor $SiCl_4$ reacted with the surface ($\equiv$) hydroxyl species. Moreover, the competition between the single bond case ($x = 1$) and multiple bonds ($1 < x \leq 3$) was directly linked to the stagnancy of precursors in the ALD regime. As far as the concentration of hydroxyl groups on the surface increased, the saturation of H_2O directly enhanced the formation of HCl. Along with the constant flow of NH_3, the ~2.2 Si/N ratio measured by XPS in the bulk of the film indicates a strong nitrogen contamination exceeding acceptable limits, especially through the inclusion of NH_4Cl salt. As indicated by George *et al.*,[31] this salt is formed as a result of the NH_3 catalyst complexing with HCl. Because of the vapour pressure of the NH_4Cl salt (*i.e.* 4×10^{-5} Torr (ref. 50)), some quantity of the salt remained within the film. In that context, note that compared to an inert gas, using NH_3 as a carrier gas may not contribute to a pure ALD process performed at RT. Indeed, a significant contamination of the surface is attributed to the excessive dose of NH_3. The contamination depicted here confirms the already described importance of adjusting the quantity of NH_3 to limit the reaction with HCl.[31] Thus, we considered that pulsing NH_3 similar to the other precursors could minimize unfavourable reactions at room temperature.

Low contamination SiO_2 growth under pulsed NH_3

Dense oxide under pure ALD regime. Based on the same chemistry used in the previous part, each chemical involved in the following process has been considered as a precursor. This indicates that an adequate separation of each pulsed chemical has been guaranteed. The purge of the reactor has been optimized using the appropriate ratio of carrier gas flow/reactor base pressure (<2 Torr). Any overlap between each precursor pulse has been prevented by checking the injection with the integrated RGA. Fig. 3 shows the ALD saturation curves at RT for $SiCl_4$ (a), H_2O (b) and NH_3 (c) precursors. According to the diagrams, the saturation of all precursors occurs after exposure for 90 s. The N_2 purging time between $SiCl_4$ and NH_3 precursors has been fixed at 90 s. The appropriate purging time after water exposure was then determined by RGA (H_2O: $m/z = 18$ uma) analysis using a systematic variation process (Fig. S4, ESI†). After 300 s purging time, water was completely removed from the reactor.

Based on the trends observed in Fig. 4, the growth of a SiO_2 film in a pure ALD regime at RT has been investigated. $SiCl_4$,
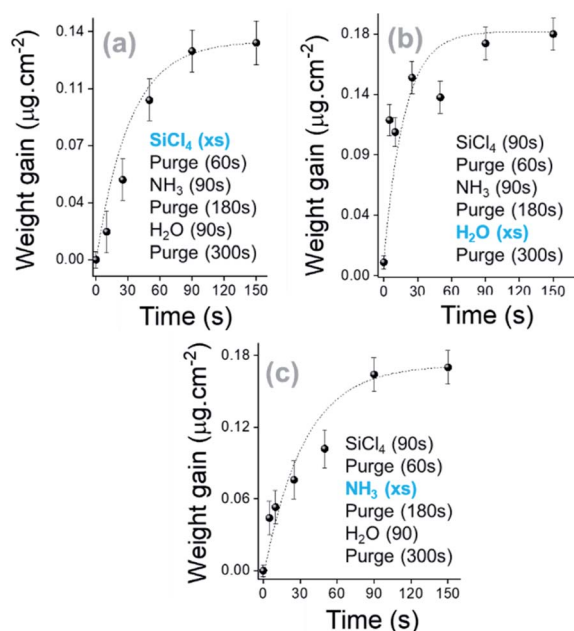
Fig. 3 Saturation curves of $SiCl_4$, H_2O and NH_3 along the SiO_2 thin film growth. The kinetic growth is shown for 5 cycles with sequential exposure of the surface.
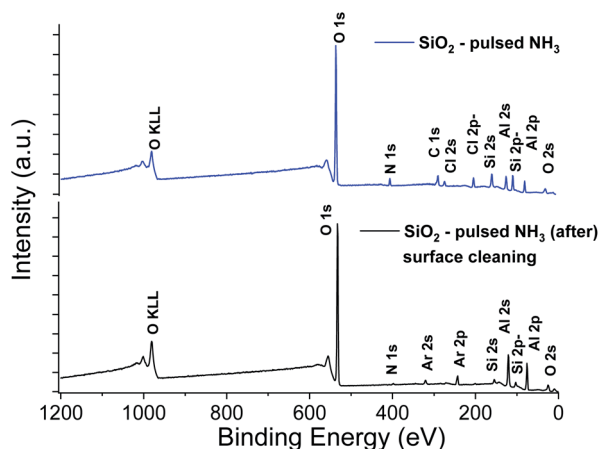

Fig. 4 XPS survey spectra of SiO_2 thin film obtained with a sequential 90 s exposure of $SiCl_4$, NH_3 and H_2O precursors. Upper panel corresponds to the signal of the raw film and lower panel to the film after surface cleaning.

NH_3 and H_2O exposure times were fixed at 90 s and extended purges were applied after NH_3 and H_2O pulses at 180 s and 300 s, respectively. As shown in Fig. S5a, ESI,† the 0.02 μg cm^{-2} per cycle weight gain is 30 times lower than the process with a constant flow of NH_3 (Fig. S2, ESI†). Nevertheless, the injection of NH_3 and H_2O precursors significantly contributes to a certain gain of mass (Fig. S5 panel b, ESI†), and then a growth rate of 0.5 Å per cycle is obtained for 500 deposition cycles. It can be observed that the high H_2O mass adsorbed during the interaction of H_2O molecules with active complexes at the

surface ends through the efficient replacement of chlorine by hydroxyl groups (Fig. S3, ESI†).

The XPS elemental analysis (Fig. 4) still shows the presence of chlorine, nitrogen and carbon in addition to silicon and oxygen. The amount of contaminants (Table 2) is nonetheless substantially decreased. Firstly, the Si/Cl ratio increased from ∼4 (surface) to ∼8.7 in the bulk of the film. Secondly, compared to the films obtained with a constant flow of ammonia, the Si/Cl ratio improved significantly (threefold). Moreover, the Si/N ratio increased from 1.1 to 3.8 (2.2 to 5.9 inside the film). This indicates a limited reaction between HCl and NH_3 to form NH_4Cl. The best fitting procedure of the high-resolution spectrum of N 1s reveals a single binding energy peak at 401.1 ± 0.3 eV, corresponding to NH_3^+. This confirms the formation of the NH_4Cl salt, and the small amount of detected Al is attributed to the alumina sub-layer (*i.e.* $SiO_2/Al_2O_3/Si$).

The SIMS depth profile of the SiO_2 film is shown in Fig. 5. The intensity of chlorine decreases ∼30 times faster than the process performed with the constant NH_3 flow. In fact, less than 100 s sputtering is needed to decrease the intensity below 1 × 10^5 cnts per s compared to ∼2800 s for the NH_3 constant flow process. Moreover, the intensity of nitrogen seems to be in the same range of 10–100 cnts per s. Compared to the XPS results, this corroborates the formation of the NH_4Cl salt. Note that the intensity of Si is higher than that of Al, confirming the coating process of SiO_2 on Al_2O_3. From the depth profile, we can estimate the SiO_2 film thickness to be around 25 nm. Based on the XPS and SIMS results, it can be assumed that this RT process is optimized in terms of surface exposure. Nevertheless, the residual traces of HCl still react with NH_3 because of the difficulties to purge H_2O or NH_3 at RT. Moreover, small quantities of byproducts, such as NH_4Cl, were consequently integrated into the film.

Fig. 6a and b show top-view SEM images of the SiO_2 film. We observed a rough layer with grain sizes of up to 200 nm. This roughness is highlighted in the 45° tilted view (Fig. 6c).

Furthermore, cross-section analyses evidence the presence of a compact film (Fig. 6d). From these pictures, we can conclude that this pulsed NH_3 growth process leads to dense but rough SiO_2 thin films. A thickness of 30 ± 5 nm is measured through the cross-section, close to the 25 nm value deduced from the SIMS analysis. This leads to a lower growth rate of ∼0.5 Å per cycle related to the lower weight gain observed with QCM (*i.e.* 30× lower than the SiO_2 film processed under a constant flow of NH_3). Nevertheless, the irregular surface aspect reveals

Table 2 XPS quantification of elements present in the SiO_2 thin film obtained with a pure ALD regime

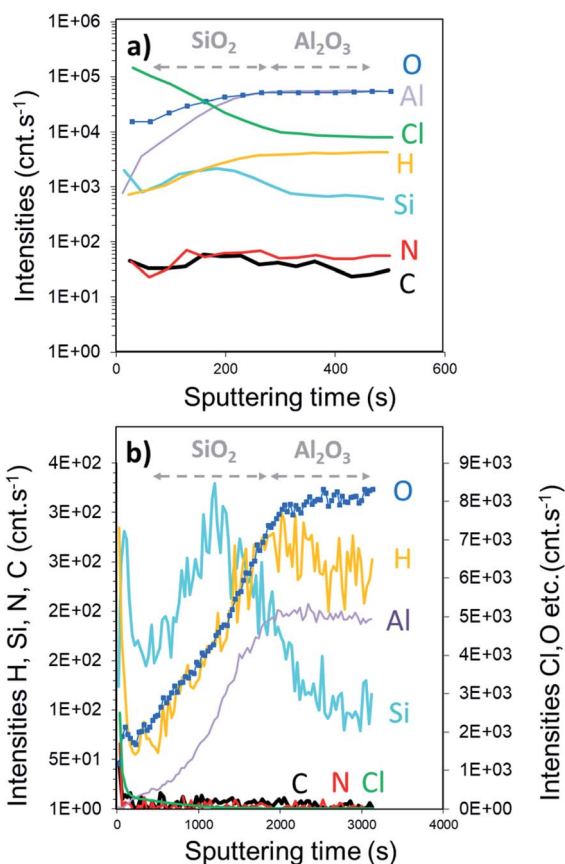| Name	At%	At% (depth profiling)
Si 2p	12.9	4.1
O 1s	54.2	59.7
N 1s	3.6	0.7
Cl 2p	3.2	0.5
C 1s	11.4	<1.0
Al 2p	14.7	34.9

Fig. 5 SIMS depth profile of pure ALD SiO$_2$ film obtained with 90 s pulse of SiCl$_4$; NH$_3$ and H$_2$O precursors and extended N$_2$ purges for 60, 180 and 300 s. Fast and slow sputtering rate are shown in panels (a) and (b), respectively.
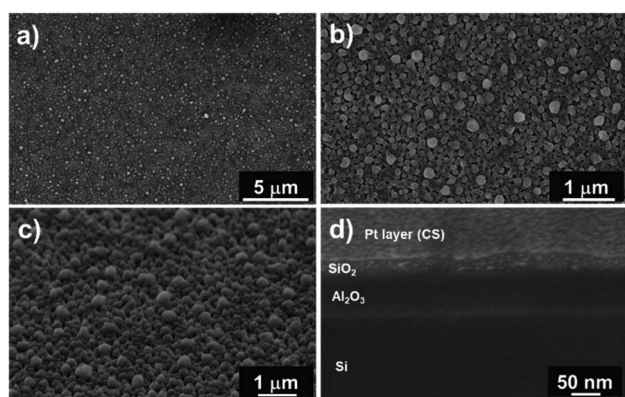

Fig. 6 SEM images of the pure ALD SiO$_2$ film processed for 500 cycles at different magnifications: (a and b) top and (c) 45° tilted view of the entire oxide film. (d) FIB cross-section images reveal a dense state of the SiO$_2$ film with an inhomogeneous crystallisation due to the inclusion of contaminants and the low growth rate of 0.5 Å per cycle.

that the process does not correspond to a pure ALD growth mode, as expected.[51–53] This peculiar non-homogeneous growth at RT suggests that the surface reaction is in competition with the integration of contaminants. The self-limiting process

actually promotes the deposition of species onto the substrate and onto the deposits (*e.g.* islands) with equal probability.[54–56] The inclusion of contaminants at a sub-atomic growth rate (*i.e.* <1 Å per cycle) could explain the morphology of the obtained film. Moreover, the high amount of –OH surface groups could affect the dehydroxylation/rehydroxylation equilibrium (section: Contaminant inclusion mechanism), leading to the production of a higher quantity of HCl in the case of trifunctional bonds. Nevertheless, the oxide thin film displays a significant density in volume with limited inhomogeneity. This is in line with the sub-atomic growth rate mechanism surrounded by limited contamination. The tailoring of ALD parameters in this RT-SiO$_2$ growth process shows a substantial adaptability in terms of morphology and chemical composition. These results suggest that a tuning of the growth parameters could influence the crystallisation. Hence, different types of SiO$_2$ layers could be processed at RT.

Porous oxide under limited ALD regime. As described in the previous section, less contaminated SiO$_2$ can be produced by adjusting the surface exposure of SiCl$_4$, NH$_3$ and H$_2$O precursors. Furthermore, the effect of limited exposure on the composition and the morphology of the film has been investigated. Hence, the process has been tuned to maintain low level of contaminants in an ALD non-saturation regime. The precursor exposure has been decreased to a minimum value for SiCl$_4$ (*i.e.* 100 ms) in agreement with a low contamination strategy. Then, according to RGA results, the exposure time of NH$_3$ and H$_2$O was fixed to 2 s for both with a purge of only 10 s using 300 sccm of N$_2$.

As shown in Fig. S6, ESI,† a growth rate of 1.54 µg cm^{-2} per cycle was obtained. Compared to the process described in the previous section, the exposure reaction used here generates ∼50 times higher weight gain. In order to disentangle any physico-chemical influence from the substrate, silicon oxide films were grown on a pre-characterized barrier layer. Hence, SiO$_2$ growth was investigated on two different sub-layers, *i.e.* TiO$_2$ deposited by ALD and Si bulk.
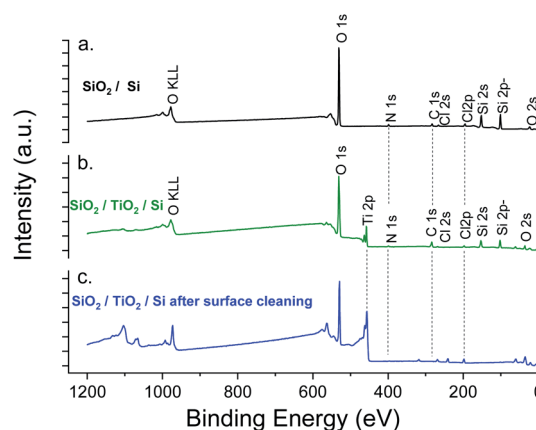

Fig. 7 XPS survey spectra of SiO$_2$ thin film obtained with a sequential exposure of SiCl$_4$, NH$_3$ and H$_2$O precursors. SiO$_2$ film deposited on (a) Si wafer, (b, c) TiO$_2$/Si (80 nm) before and after surface cleaning respectively.

Fig. 7 shows the XPS experiment results. As expected, Cl, C, N elements were detected in both samples. For SiO_2 deposited on TiO_2, the detection of Ti 2p before etching confirms the low thickness of the film.

However, the percentage of chlorine was clearly maintained below the limit of 3% (obtained for the previous process with extended exposures) (Table 3). The higher chlorine concentration observed after etching (3.79 at%) was attributed to the chlorine inherent to the TiO_2 ALD process. This was confirmed by the low chlorine concentration for SiO_2 deposited directly on the silicon wafer (Table 3, SiO_2/Si). In order to screen the composition and morphology of the film, thicker SiO_2 layer (2500 cycles) were processed on a chlorine-free material, *i.e.* Al_2O_3 (50 nm) on Si.

The SIMS depth profiling of the synthesized SiO_2 thick film exhibits a concentration of chlorine that rapidly decreases as a function of sputtering time (Fig. 8). Compared to the previous process, the intensity of Cl is starting a decade less, around 3.5 $\times 10^4$ cnts per s. Moreover, the amount of C and N is very low, which confirms the low level of NH_4Cl contamination in a thick volume of SiO_2.

Furthermore, the higher concentration of chlorine close to the surface of the film indicated the slow dissociative chemisorption of water, which induced the desorption of HCl. This recombination clearly affected the growth mechanism of SiO_2. As shown in Fig. 9, SEM analyses highlighted the porous state of the oxide film. In addition to the 200–500 nm diameter aggregates on the surface of the layer, the top and tilted view (Fig. 9a) revealed a SiO_2 sponge-like structure. The porosity of the film was confirmed by SAXS where a periodical arrangement of pores could be fitted with an average radius of 130 Å (std dev 30% and most frequent radius ∼ 110 Å). The applied FIB cross-section (Fig. 9b) reveals the presence of 20–50 nm cavities (merging pores due to the preparation) and isolated pores of ∼15 nm. As explained by Puurunen in the ALD random deposition approach,[56] if the growth per cycle is not constant, the increase in the surface roughness should be fast at the beginning of the
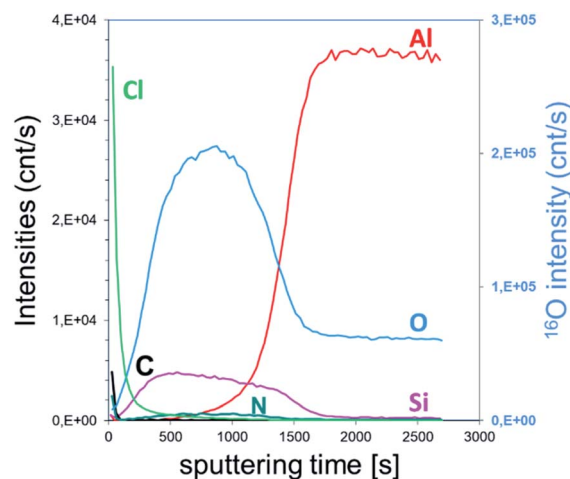

Fig. 8 SIMS depth profile of porous SiO_2 film obtained with 100 ms pulse of $SiCl_4$, 2s of NH_3 and H_2O precursors.

growth and slow thereafter. This naturally indicates that a smaller number of ALD reaction cycles are required to fit a conformal deposition in a close-packed array as far as the growth rate is adjacent to an atomic monolayer.

By considering the growth rate of ∼0.11 Å per cycle obtained in this process, it could explain why the SiO_2 film is less "closed" as the one processed *via* the pure ALD approach. The sponge-like porous structure growth may be related to the limited surface diffusion of the by-products (NH_4Cl, HCl) generated during each half cycle. Indeed, the diffusion/desorption of byproducts is slower in the case of low reaction temperature

Table 3 XPS quantification of the suitable elements of the SiO_2 thin film obtained with an optimized ALD regime on a TiO_2/Si substrate and a Si substrate

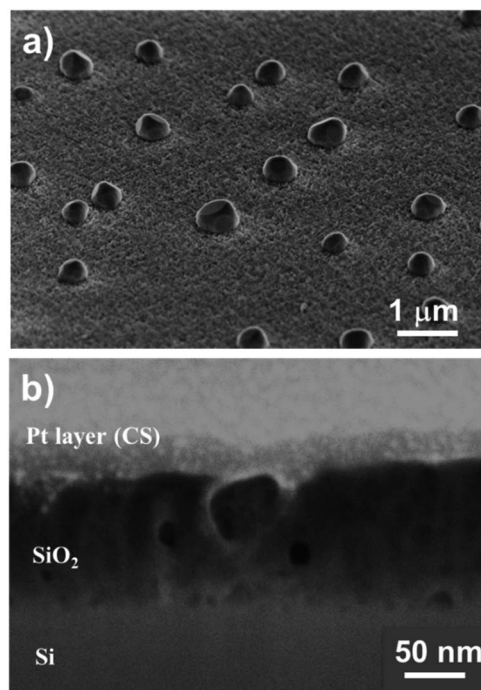| Name	At%	At% (depth profiling)
SiO_2/TiO_2/Si		
Si 2p	16.4	—
O 1s	58.8	63.4
N 1s	1.4	—
Cl 2p	1.1	3.8
C 1s	14.6	—
Ti 2p	7.7	32.8
SiO_2/Si		
Si 2p	25.9	34.4
O 1s	60.5	62.9
N 1s	1.6	2.3
Cl 2p	1.0	0.5
C 1s	11.1	<1

Fig. 9 SEM images of the ∼260 nm thick ALD SiO_2 (300 cycles) film at different magnifications: (a) 45° tilted view of the entire oxide film; (b) FIB cross-section that confirms the porous state of the film.
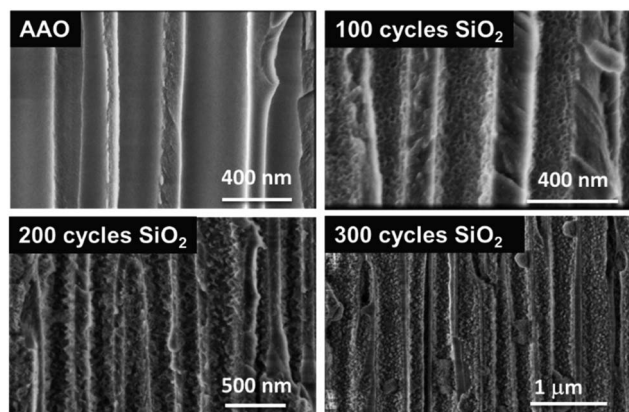
Fig. 10 SEM images of ALD grown SiO$_2$ films with various thicknesses (100–300 cycles) deposited in AAO membranes.

(here RT) and short purge time. In this case, residual water or byproducts (NH$_4$Cl, HCl) are considered as surface fractions where the supplementary amount of the injected precursor will be adsorbed instead of the –Si–OH surface groups. This prevents the growth of SiO$_2$ and leads to non-uniform porous thin films. Nevertheless, this peculiar structure is very attractive for applications that need to be processed at RT. Even if other techniques such as PE-ALD are able to produce SiO$_2$ dense thin films with no impurities at reduced temperatures (50–80 °C) for specific applications,[41–43,57] we evidenced our ability to fabricate a highly porous SiO$_2$ layer at room temperature with a significant level of control of the contamination. This specific characteristic of this porous SiO$_2$ layer is clearly transferred to complex and temperature-sensitive 3D materials. Hence, ALD SiO$_2$ could be deposited in a porous anodic aluminum oxide (AAO) membrane, and the results are shown in Fig. 10. It clearly appears that the porosity obtained on planar substrates is perfectly transferable to 3D surfaces. This suggests that the ALD technique for SiO$_2$ thin film synthesis could be applied to any 3D complex substrate. Further studies are in progress.

Conclusions

Porous SiO$_2$ thin films have been produced by ALD using a sequential exposure of SiCl$_4$, NH$_3$ and H$_2$O at room temperature. The catalytic effect of ammonia has been exploited to optimize the saturation of the precursors and the extended purges. A relation between the significant porosity and the chemical saturation of the surface has been indicated using QCM, XPS, SIMS and SEM. It has also been demonstrated that this optimized process exhibited a decrease in the inherent inclusion of contaminants such as NH$_4$Cl and HCl in the film. As demonstrated on AAO membranes, the transferability of this 2D process to 3D structures could extend the use of SiO$_2$ films in several domains such as complex or high aspect ratio materials.

Conflicts of interest

The authors disclose that there are there are no conflicts to declare.

Acknowledgements

References

1 C. J. Frosch and L. Derick, Surface Protection and Selective Masking during Diffusion in Silicon, *J. Electrochem. Soc.*, 1957, **104**(9), 547–552.

2 S. Wolf and R. N. Tauber, *Deep Sub-micron process technology*. Lattice Press, CA, 1986.

3 C. O. A. Olsson and D. Landolt, Passive films on stainless steels chemistry, structure and growth, *Electrochim. Acta*, 2003, **48**(9), 1093–1104.

4 C. G. Granqvist, Transparent conductors as solar energy materials: A panoramic review, *Sol. Energy Mater. Sol. Cells*, 2007, **91**(17), 1529–1598.

5 J. A. Howarter and J. P. Youngblood, Self-Cleaning and Anti-Fog Surfaces *via* Stimuli-Responsive Polymer Brushes, *Adv. Mater.*, 2007, **19**(22), 3838–3843.

6 T. Kako, *et al.*, Adhesion and sliding of wet snow on a super-hydrophobic surface with hydrophilic channels, *J. Mater. Sci.*, 2004, **39**(2), 547–555.

7 L. Y. L. Wu, *et al.*, Quantitative test method for evaluation of anti-fingerprint property of coated surfaces, *Appl. Surf. Sci.*, 2011, **257**(7), 2965–2969.

8 P. Ragesh, *et al.*, A review on self-cleaning and multifunctional materials', *J. Mater. Chem. A*, 2014, **2**(36), 14773–14797.

9 H. K. Park, S. W. Yoon and Y. R. Do, Superhydrophobicity of 2D SiO$_2$ hierarchical micro/nanorod structures fabricated using a two-step micro/nanosphere lithography, *J. Mater. Chem.*, 2012, **22**(28), 14035–14041.

10 Y. Gao, *et al.*, Highly Transparent and UV-Resistant Superhydrophobic SiO2-Coated ZnO Nanorod Arrays, *ACS Appl. Mater. Interfaces*, 2014, **6**(4), 2219–2223.

11 B. Xu, *et al.*, Preparation of superhydrophobic cotton fabrics based on SiO$_2$ nanoparticles and ZnO nanorod arrays with subsequent hydrophobic modification, *Surf. Coat. Technol.*, 2010, **204**(9–10), 1556–1561.

12 Y. Zheng, *et al.*, Formation of SiO$_2$/polytetrafluoroethylene hybrid superhydrophobic coating, *Appl. Surf. Sci.*, 2012, **258**(24), 9859–9863.

13 J. W. Klaus, O. Sneh and S. M. George, Growth of SiO$_2$ at Room Temperature with the Use of Catalyzed Sequential Half-Reactions, *Science*, 1997, **278**(5345), 1934–1936.

14 C. C. Fulton, G. Lucovsky and R. J. Nemanich, Process-dependent band structure changes of transition-metal (Ti,Zr,Hf) oxides on Si (100), *Appl. Phys. Lett.*, 2004, **84**(4), 580–582.

15 X. Wang, *et al.*, Comprehensive understanding of the effect of electric dipole at high-k/SiO$_2$ interface on the flatband voltage shift in metal-oxide-semiconductor device, *Appl. Phys. Lett.*, 2010, **97**(6), 062901–062903.

16 K. Kita and A. Toriumi, Origin of electric dipoles formed at high-k/SiO$_2$ interface, *Appl. Phys. Lett.*, 2009, **94**(13), 132902–132903.

17 X. Wang, *et al.*, Electric Dipole at High-k/SiO$_2$ Interface and Physical Origin by Dielectric Contact Induced Gap States, *Jpn. J. Appl. Phys.*, 2011, **50**(10), 10PF02.

18 C. Kirkpatrick, *et al.*, Performance improvement of AlGaN/GaN high electron mobility transistors with atomic layer deposition (ALD) of SiO$_2$ and HfAlO dielectrics, *Phys. Status Solidi C*, 2011, **8**(7–8), 2445–2447.

19 B. Lee, *et al.*, Normally-off AlGaN/GaN MOSHFET using ALD SiO$_2$ tunnel dielectric and ALD HfO$_2$ charge storage layer for power device application, *Phys. Status Solidi C*, 2012, **9**(3–4), 868–870.

20 G. Dingemans, M. C. M. van de Sanden and W. M. M. Kessels, Excellent Si surface passivation by low temperature SiO$_2$ using an ultrathin Al$_2$O$_3$ capping film, *Phys. Status Solidi RRL*, 2011, **5**(1), 22–24.

21 G. Dingemans, *et al.*, Controlling the fixed charge and passivation properties of Si(100)/Al$_2$O$_3$ interfaces using ultrathin SiO$_2$ interlayers synthesized by atomic layer deposition, *J. Appl. Phys.*, 2011, **110**(9), 093715–093716.

22 G. Dalapati, *et al.*, Surface Passivation of GaAs Substrates with SiO$_2$ Deposited Using ALD, *Electrochem. Solid-State Lett.*, 2011, **14**(10), G52–G55.

23 H. Guo, *et al.*, High-performance GaN-based light-emitting diodes on patterned sapphire substrate with a novel hybrid Ag mirror and atomic layer deposition-TiO$_2$/Al$_2$O$_3$ distributed Bragg reflector backside reflector, *Opt. Eng.*, 2013, **52**(6), 063402.

24 H. Kim and P. McIntyre, Atomic Layer Deposition of Ultrathin Metal-Oxide Films for Nano-Scale Device Applications, *J. Korean Phys. Soc.*, 2006, **48**, 5–17.

25 L. Giordano and G. Pacchioni, Oxide Films at the Nanoscale: New Structures, New Functions, and New Materials, *Acc. Chem. Res.*, 2011, **44**(11), 1244–1252.

26 K. E. Elers, *et al.*, Film Uniformity in Atomic Layer Deposition, *Chem. Vap. Deposition*, 2006, **12**(1), 13–24.

27 S. M. George, Atomic Layer Deposition: An Overview, *Chem. Rev.*, 2009, **110**(1), 111–131.

28 H. Kim and P. C. McIntyre, Atomic layer deposition of ultrathin metal-oxide films for nano-scale device applications, *J. Korean Phys. Soc.*, 2006, **48**(1), 5–17.

29 J. D. Ferguson, *et al.*, ALD of SiO at Room Temperature Using TEOS and H$_2$O with NH$_3$ as the Catalyst, *J. Electrochem. Soc.*, 2004, **151**(8), G528–G535.

30 J. W. Klaus, *et al.*, Atomic layer deposition of SiO$_2$ using catalysed and uncatalysed self-limiting surface reactions, *Surf. Rev. Lett.*, 1999, **6**(3–4), 435–448.

31 J. W. Klaus and S. M. George, Atomic layer deposition of SiO$_2$ at room temperature using NH$_3$-catalyzed sequential surface reactions, *Surf. Sci.*, 2000, **447**(1–3), 81–90.

32 B. A. McCool and W. J. DeSisto, Self-Limited Pore Size Reduction of Mesoporous Silica Membranes *via* Pyridine-Catalyzed Silicon Dioxide ALD, *Chem. Vap. Deposition*, 2004, **10**(4), 190–194.

33 B. A. McCool and W. J. DeSisto, Synthesis and Characterization of Silica Membranes Prepared by Pyridine-Catalyzed Atomic Layer Deposition, *Ind. Eng. Chem. Res.*, 2004, **43**(10), 2478–2484.

34 W. Gasser, Y. Uchida and M. Matsumura, Quasi-monolayer deposition of silicon dioxide, *Thin Solid Films*, 1994, **250**(1–2), 213–218.

35 S. Morishita, Y. Ushida and M. Matsumura, Atomic-Layer Chemical-Vapor-Deposition of SiO$_2$ by Cyclic Exposures of CH$_3$OSi(NCO)$_3$ and H$_2$O$_2$, *Jpn. J. Appl. Phys.*, 1995, **34**, 5738–5742.

36 S. Morishita, *et al.*, New substances for atomic-layer deposition of silicon dioxide, *J. Non-Cryst. Solids*, 1995, **187**, 66–69.

37 M. Degai, *et al.*, Non-heating atomic layer deposition of SiO$_2$ using tris(dimethylamino)silane and plasma-excited water vapor, *Thin Solid Films*, 2012, **525**, 73–76.

38 J. Lim, S. Yun and J. Lee, Low-Temperature Growth of SiO$_2$ Films by Plasma-Enhanced Atomic Layer Deposition, *ETRI Journal*, 2005, **27**(1), 118–121.

39 B. B. Burton, *et al.*, Rapid SiO$_2$ Atomic Layer Deposition Using Tris(*tert*-pentoxy)silanol, *Chem. Mater.*, 2008, **20**(22), 7031–7043.

40 T. Nam, *et al.*, Low-temperature, high-growth-rate ALD of SiO$_2$ using aminodisilane precursor, *Appl. Surf. Sci.*, 2019, **485**, 381–390.

41 J. Sheng, *et al.*, Performance and Stability Enhancement of In–Sn–Zn–O TFTs Using SiO$_2$ Gate Dielectrics Grown by Low Temperature Atomic Layer Deposition, *ACS Appl. Mater. Interfaces*, 2017, **9**(49), 42928–42934.

42 J.-H. Lee, *et al.*, Plasma enhanced atomic layer deposited silicon dioxide with divalent Si precursor [*N,N′-tert*-butyl-1,1-dimethylethylenediamine silylene], *Appl. Surf. Sci.*, 2019, **493**, 125–130.

43 Y. Lee, *et al.*, Effects of O$_2$ plasma treatment on moisture barrier properties of SiO$_2$ grown by plasma-enhanced atomic layer deposition, *Ceram. Int.*, 2019, **45**(14), 17662–17668.

44 G. Dingemans, *et al.*, Plasma-Assisted ALD for the Conformal Deposition of SiO$_2$: Process, Material and Electronic Properties, *J. Electrochem. Soc.*, 2012, **159**(3), H277–H285.

45 D. Hiller, *et al.*, Low temperature silicon dioxide by thermal atomic layer deposition: Investigation of material properties, *J. Appl. Phys.*, 2010, **107**(6), 064314.

46 Y. Du, X. Du and S. M. George, SiO$_2$ film growth at low temperatures by catalyzed atomic layer deposition in a viscous flow reactor, *Thin Solid Films*, 2005, **491**(1–2), 43–53.

47 H.-U. Kim and S.-W. Rhee, Electrical Properties of Bulk Silicon Dioxide and SiO$_2$/Si Interface Formed by Tetraethylorthosilicate-Ozone Chemical Vapor Deposition, *J. Electrochem. Soc.*, 2000, **147**(4), 1473–1476.

48 O. Sneh, *et al.*, Atomic layer growth of SiO$_2$ on Si(100) using SiCl$_4$ and H$_2$O in a binary reaction sequence, *Surf. Sci.*, 1995, **334**(1–3), 135–152.

49 D. Damyanov, *et al.*, On the mechanism of interaction between TiCl$_4$ vapour and surface OH groups of

amorphous SiO_2, *J. Non-Cryst. Solids*, 1988, **105**(1–2), 107–113.

50 *CRC Handbook of Chemistry and Physics*, CRC Press, Boca Raton, FL, 63rd edn 1984.

51 T. Suntola, Atomic layer epitaxy, *Mater. Sci. Rep.*, 1989, **4**(5), 261–312.

52 T. Suntola, Atomic layer epitaxy, *Thin Solid Films*, 1992, **216**(1), 84–89.

53 M. Ritala, *et al.*, Perfectly Conformal TiN and Al_2O_3 Films Deposited by Atomic Layer Deposition, *Chem. Vap. Deposition*, 1999, **5**(1), 7–9.

54 Y. Kajikawa, S. Noda and H. Komiyama, Use of process indices for simplification of the description of vapor deposition systems, *Mater. Sci. Eng., B*, 2004, **111**(2–3), 156–163.

55 R. L. Puurunen, Formation of metal oxide particles in atomic layer deposition during the chemisorption of metal chlorides: A review, *Chem. Vap. Deposition*, 2005, **11**(2), 79–90.

56 R. L. Puurunen, Random Deposition as a Growth Mode in Atomic Layer Deposition, *Chem. Vap. Deposition*, 2004, **10**(3), 159–170.

57 Y.-J. Choi, *et al.*, Robust SiO_2 gate dielectric thin films prepared through plasma-enhanced atomic layer deposition involving di-sopropylamino silane (DIPAS) and oxygen plasma: Application to amorphous oxide thin film transistors, *Ceram. Int.*, 2018, **44**(2), 1556–1565.

58 K. Pfeiffer, Comparative study of ALD SiO_2 thin films for optical applications, *Opt. Mater. Express*, 2016, **6**(2), 660–670, https://www.osapublishing.org/ome/abstract.cfm?URI=ome-6-2-660.

59 V. Beladiya, Effect of an electric field during the deposition of silicon dioxide thin films by plasma enhanced atomic layer deposition: an experimental and computational study, *Nanoscale*, 2020, **12**(3), 2089–2102.

60 P. Paul, Antireflection Coating on PMMA Substrates by Atomic Layer Deposition, *Coatings*, 2020, **10**(1), 64–77, https://www.mdpi.com/2079-6412/10/1/64.